Anomalous lepton acceleration in the radiation reaction dominated reflection regime

Xiaofei Shen ,[*,†] Yue-Yue Chen,[‡] Karen Z. Hatsagortsyan ,[§] and Christoph H. Keitel
Max-Planck-Institut für Kernphysik, Saupfercheckweg 1, 69117 Heidelberg, Germany

(Received 14 April 2025; revised 22 October 2025; accepted 22 January 2026; published 18 March 2026)

Relativistic electrons colliding with intense counterpropagating laser pulses are expected to lose energy through radiation reaction. However, we reveal a counterintuitive regime where reflected leptons (including incident electrons, generated electrons, and positrons) gain significant energies when an ultraintense laser pulse interacts with counterpropagating electrons. Because of strong radiation reaction, these particles can be halted and reflected near the laser peak. The subsequent asymmetric laser field then accelerates the reflected leptons to energies far exceeding their initial values. Using three-dimensional particle-in-cell simulations, we demonstrate the generation and acceleration of quasimonoenergetic positrons to multi-GeV energies with a high number conversion efficiency employing forthcoming multipetawatt lasers, which provide conceptually a simple single-stage solution for positron creation and acceleration. The proposed mechanism of lepton acceleration is scalable to the astrophysical scenario and can be related to the origin of ultrahigh-energy cosmic rays in environments with intense fast radio bursts.

DOI: 10.1103/bc2k-5d5m

I. INTRODUCTION

Laser-driven particle accelerators have attracted significant attention because of their ability to sustain orders of magnitude larger acceleration gradients compared to conventional radio-frequency-based systems. In particular, laser wakefield acceleration (LWFA) has achieved remarkable success in the past decades [1–7]. While LWFA is favorable for electron acceleration, with longitudinally accelerating and transversely confining electrons, it presents notable challenges for positron acceleration, as the same fields that confine electrons tend to defocus positrons [8,9]. On the other hand, unlike electrons, positrons have to be injected externally [10–15], yet providing the required positron sources is very challenging even for conventional methods [16]. To overcome this, recently, various methods for simultaneously generating and accelerating positrons have been proposed [17–31]. However, they typically require multiple lasers and particle beams in delicate configurations [18–27], and their efficiency is generally low or difficult to scale [28–31]. Currently, despite decades of intensive research, a simple and efficient method for positron generation and acceleration remains an outstanding challenge. Therefore, positron sources are regarded as a critical milestone in the development of plasma-based acceleration with broad applications in particle physics [32], nuclear physics [33], and astrophysics [34].

On the other hand, it is well known that a free lepton cannot gain or lose energy by interacting with a plane electromagnetic wave because of the restriction of the energy-momentum conservation law (Lawson-Woodward theorem), or in more intuitive terms, because of the symmetry of the electron acceleration and deceleration in adjacent laser half cycles. However, the latter strict condition can be circumvented when the interaction in the vacuum is limited in space-time via using tightly focused or tailored laser pulses, introducing asymmetry between the laser phase-dependent acceleration-deceleration, and giving rise to the vacuum laser acceleration (VLA) mechanism [35–41]. The ponderomotive scattering [42] can significantly support the acceleration asymmetry [43–48].

The symmetry of interaction of a free electron with a laser is naturally violated during the strong-field ionization when the electron instantly appears at rest in a certain laser phase after ionization from an atom (ion) [49,50]. The ionized electron in a plane wave asymptotically moves with a transverse momentum (with respect to the laser propagation direction) determined by the vector potential of the laser field at the ionization phase ϕ_i, $p_\perp = -A(\phi_i)$, and with the corresponding longitudinal one in the relativistic case $p_\parallel = p_\perp^2/(2m)$ [51], ideally gaining an energy $\Delta\varepsilon = ma_0^2/2$, being quite significant in the relativistic laser fields [50–56], e.g., reaching 12 GeV with state-of-the-art laser intensities $\sim 10^{23}$ W/cm^2 ($a_0 \approx 220$, wavelength $\lambda_L = 800$ nm) [57]. Here, $a_0 = eE_L/(m\omega_L)$ is the normalized laser vector potential, with the laser field amplitude E_L, frequency ω_L, and wavelength λ_L, and the electron mass m and charge $-e$ (relativistic units $\hbar = c = 1$ are used throughout). The high acceleration gradient and simplicity of VLA have spurred significant efforts to verify and improve its performance. Nevertheless, achieving a high-quality accelerated beam via the

[*]Contact author: xfshen@pku.edu.cn
[†]Present address: Peking University, Beijing, China.
[‡]Present address: Department of Physics, Shanghai Normal University, Shanghai 200234, China.
[§]Contact author: k.hatsagortsyan@mpi-hd.mpg.de

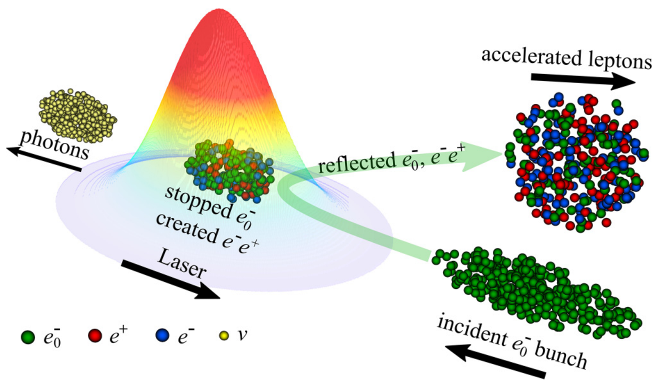

FIG. 1. Schematic setup for acceleration in the radiation reaction dominated reflection regime. A high-energy electron beam collides with an intense laser wave. Due to nonlinear Compton scattering, γ photons are emitted and electrons are stopped inside the wave. The emitted γ-rays decay into pairs due to nonlinear BW process. The stopped electrons and newborn pairs are further accelerated by the laser wave in the reflected direction to energies far exceeding the initial electron energy.

VLA is still quite challenging. Only recently, few experiments using delicate setups to facilitate sizable injection with a plasma mirror [39], thin solid foil [40], or nanotip [41], were able to generate high electron flux though with energies limited to tens of MeV.

As the laser intensity exceeds 10^{22} W/cm^2, radiation reaction (RR) effects [51,58–64], as well as positron generation due to the nonlinear Breit-Wheeler (BW) mechanism [65,66] in the laser-electron collision start to play a role (see also Refs. [67,68]). In typical setups the regime with electron γ factor $\gamma_e \gg a_0$ is considered, aimed at achieving a higher quantum nonlinearity parameter $\chi_e = E'/E_{\rm cr}$ [65], where $E' \approx \gamma_e E_L$ is the field in the electron rest frame, and $E_{\rm cr} = m^2/e$ the QED critical field. Then, the generated photons and positrons (with energies determined by the photon energy) move in the electron forward direction. However, in the case of $\gamma_e \sim a_0$, an unusual, so-called reflection regime arises, wherein the initially counterpropagating electron moves backward after the interaction due to RR [69]. The reflection regime has been employed to generate attosecond γ-rays [70,71], to polarize the reflected electrons [72], and to demonstrate the collective QED signatures of generated pair plasma [63]. In principle, strong RR can halt a counterpropagating electron (positron) in the laser field, creating dynamics similar to ionization and potentially leading to acceleration to much higher energies than the injected values. Yet, this regime has not been demonstrated, even numerically.

On another front, the universe abounds with electromagnetic radiation across the spectrum from radio waves [73] to γ-rays [74]. Near their source, the radio waves can be ultrarelativistic and potentially generate ultrahigh-energy cosmic rays (UHECRs), the origin of which remains one of the most intriguing questions in astrophysics [75].

In this paper, we put forward an acceleration method for leptons, employing the reflection regime in the setup of counterpropagating ultrastrong laser and relativistic electron beams in the RR dominated regime (Fig. 1). Acceleration of the incident electrons, and created electrons and positrons via the nonlinear BW process, are discussed. Our three-dimensional (3D) particle-in-cell (PIC) simulations demonstrate that the acceleration is especially advantageous for positrons. By colliding feasible LWFA electron beams with ultraintense lasers positron beams with energies of several GeV (about ten times higher than the initial electron energy) and high number conversion efficiency (CE) can be obtained. We explore the relevance of this scheme also for astrophysical scenarios.

II. REFLECTION ACCELERATION WITH ULTRAINTENSE LASERS

To validate the fundamental concept of reflection acceleration, we conducted 3D PIC simulations using the WarpX code [6,76–78]. The laser intensity and the electron initial energy are chosen to fulfill the reflection condition inside the laser beam $\gamma_{e0} \sim a_0$, ensure the RR dominated regime $\alpha a_0 \gtrsim 1$ [51] in the quantum regime $\chi_e \gtrsim 1$, which enable copious pair creation [65], where α is the fine-structure constant, and $\chi_e \sim 2\gamma_{e0} a_0 \omega_L/m$. These conditions during the interaction are fulfilled when we use $a_0 = 550$ (the intensity of 4×10^{23} W/cm^2), and the initial Lorentz factor $\gamma_{e0} = 10^3$. The laser field with $\lambda_L = 1$ µm is x polarized, and loosely focused with a beam waist of $w_L = 3.4$ µm, and pulse duration 25 fs [79]. The electron beam has a longitudinally uniform and transversely Gaussian density distribution. The beam length is $L_e = 10$ µm, and the transverse width $\sigma = 0.7$ µm. The maximum electron density is $n_{e_0} = 0.016 n_c$ (the initial electron number $N_e = 5 \times 10^8$). The initial energy spread is 5% and angular divergence 1 mrad. These electron beam parameters are typical for LWFA [6]. The underdense and nonrelativistic plasma due to the background gas at the electron beam exit of the LWFA stage is expected not to significantly affect the interaction. The feasibility of such a colliding regime has been demonstrated experimentally at lower a_0 [59,60,64], accounting for spatial and temporal synchronizations as well as prepulse effects. Mitigating these effects for PW lasers is discussed in Refs. [80–82], and the prepulse can be strongly suppressed by using a plasma mirror [83]. The simulation box is $60 \times 60 \times 30\lambda_L^3$, containing $360 \times 360 \times 1496$ cells, respectively, with 64 macroparticles per cell. A moving window along the laser propagation direction is employed.

The collision of the high-energy electrons with an intense laser beam (see Fig. 2) occurs at $t = 10T_L$ ($T_L = 2\pi/\omega_L$), while copious positrons begin to be created around $15T_L$. Shortly afterward they are reflected and accelerated by the laser field. Their spatial phase space distributions at $t = 15T_L$ and $30T_L$ are shown in Fig. 2. In Fig. 3(a), one representative particle is selected to illustrate the whole processes including the collision (green), photon radiation (black arrow), pair generation (red for positrons and blue for electrons), and lepton acceleration.

During the collision, a significant number of high-energy photons (about 4×10^7 photons with energy above 10 MeV) is emitted via nonlinear Compton scattering. The emitted photons move along the same direction as the initial electron beam, and further collide with the laser pulse near the peak, leading to substantial pair production, as the photon quantum strong-field parameter $\chi_\gamma \sim \chi_e \sim 1$. Initially, the created

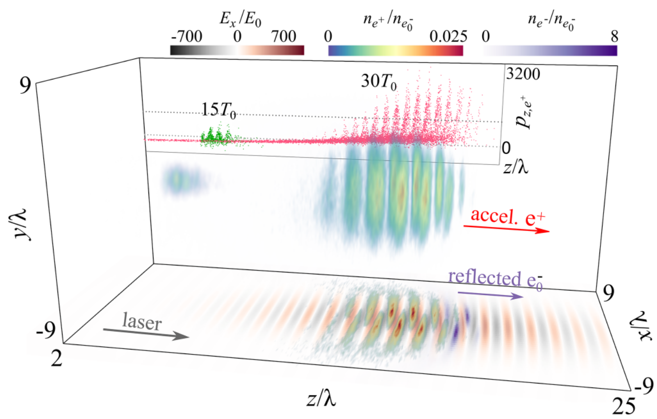

FIG. 2. Creation, reflection, and acceleration of positrons. Their number density distribution in space is represented by the blue-green-red color map, while their phase spaces (p_{z,e^+}, z) (green dots for $t = 15T_L$ and red for $30T_L$) are displayed at the back surface (the dotted line corresponds to the electron initial momentum). The slices of the laser field with $E_0 = m\omega_L/e$ and reflected electron beam density are illustrated by the gray-brown and purple color map, respectively.

pairs move backwards [see the insets of Figs. 2 and 3(a)]. Then, due to the RR and Lorentz force, almost all electrons and generated pairs are reflected by the laser pulse. The positrons after the interaction mostly have nonvanishing transverse momentum p_x correlated with the laser vector potential at the creation point [see the insets of Fig. 3(b)]. The reflected leptons are compressed in the longitudinal direction, while

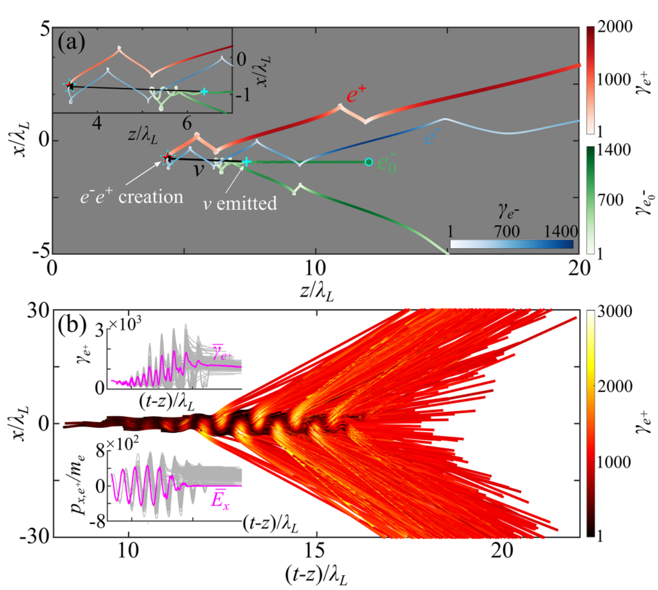

FIG. 3. Particle trajectories. (a) Illustration of generation and acceleration processes of a typical pair, where the green cross and red asterisk mark the places where the photon with an energy of 162.5 MeV ($\chi_\nu \approx 0.8$) is emitted and the pair is generated, respectively. (b) Trajectories of positrons in the comoving frame, randomly selected with $\gamma_{e^+} > 1000$ at $t = 60\,T_L$. Insets show the evolution of the positrons γ_{e^+} (upper) and $p_{x,e^+} > 0$ (lower) with final $p_{x,e^+} > 0$. The magenta line in the upper inset represents the average $\overline{\gamma}_{e^+}$, while the lower shows the average $\overline{E}_x$.

spreading in the transverse direction due to the unavoidable ponderomotive scattering. The peak positron density reaches about $0.3n_{e0}$ and then slowly decreases to be about $0.025n_{e0}$ at $t = 30T_L$ due to the transverse expansion, as shown in Fig. 2.

While here we consider a relatively loosely focused laser pulse, the dephasing time of the accelerated leptons is much longer than the time it takes for them to exit the focal volume transversely (see the Appendix). As a result, the acceleration primarily ceases when the leptons leave the focal volume [Fig. 2(b)], and their final energies can be lower than the theoretical prediction with a plane wave. Examples of acceleration parameters with $a_0 = 550$ and $a_0 = 1000$ are given in Fig. 4. The net maximum energy $\mathcal{E}_{\max}$ at $a_0 = 550$ ($a_0 = 10^3$) reaches about 2.5 GeV (6 GeV), about five times (12 times) higher than the injected electron energy. The energy spectra of the injected electrons, created electrons and positrons are similar and their maximum energies are comparable. The beam charge of the reflected positrons is about 10 pC (68 pC), leading to a number conversion efficiency (CE) from electron to positron of about 12.5% (85%). Selecting positrons within 12.5° (4.5°), a quasimonoenergetic beam with a peak energy of about 0.82 GeV (2.8 GeV) can be obtained [see the insets of Figs. 4(b) and 4(d)]. At $a_0 = 10^3$ nearly an equivalent number of pairs with the initial electrons is obtained, and it can be further enhanced with higher a_0 or γ_{e0}. Interestingly, the maximum energies of the pairs are larger than those of the initial electrons, because most electrons are stopped before reaching the peak of the laser pulse, while the emitted photons can reach the peak and generate pairs with a larger acceleration.

With the increase of the laser intensity, the RR force becomes dominant over the ponderomotive force. The Particles' transverse motion is strongly suppressed and then the dephasing length becomes longer. They will have a larger chance to stay in the same half laser cycle before moving out of the laser focal spot (see the Appendix). Therefore, more leptons will be accelerated to higher energies, leading to a flatter energy spectrum in Fig. 4(c) and their divergence also becomes much smaller [Fig. 4(d)]. We give a simple estimation about the maximum particle energy at reasonable yield obtained in a laser wave with finite spot size w_L in the RR dominated regime (see the Appendix),

$$\mathcal{E}_{\max} \approx \pi m a_0 \frac{w_L}{\lambda_L} \approx 400\sqrt{\frac{P_w}{\mathrm{PW}}}\ \mathrm{MeV}, \tag{1}$$

where P_w is the laser power in units of PW. The energy gain of the reflected leptons is proportional to w_L, because the actual acceleration is in the transverse direction due to the transverse character of the laser field. On the other hand, the RR force, determined by a_0, is inversely proportional to w_L at the given power of the laser pulse. Consequently, the final energy gain depends only on the laser power as highlighted by Eq. (1). Thus, the energy gain in the considered scheme does not critically depend on the focusing conditions. We underline that the reflection regime is suitable for generating and accelerating positrons in a single stage, whereas in LWFA positrons have to be injected from another source and a special setup is required to suppress defocusing during acceleration [9], even though it promises higher energies for electrons under current laser conditions.

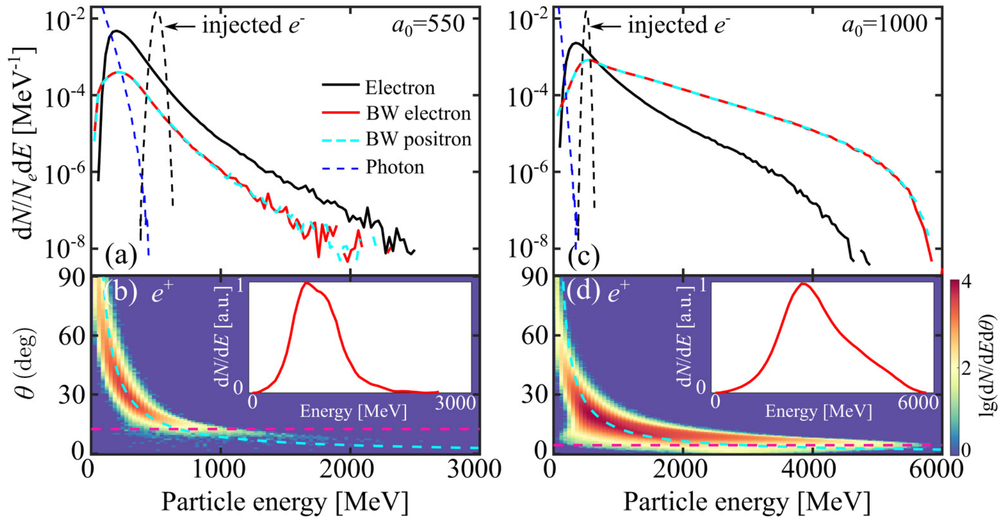

FIG. 4. Energy spectra [(a), (c), normalized to N_e] and angular distribution [(b), (d)] obtained with $a_0 = 550$ [(a), (b)] and 1000 [(c), (d)]. Here particles are collected at simulation boundaries. Insets in (b), (d) present the energy spectra of positrons selected within 12.5° and 4.5° (marked by the magenta horizontal dashed lines), respectively. The black dashed lines in (a) and (c) show the energy spectrum of injected electrons, while the cyan dashed lines in (b) and (d) show a θ^{-1} dependence predicted by Eq. (2), where $\theta = \arctan(p_\perp/p_z)$.

To validate the scaling law, we have conducted more 3D simulations by varying a_0 and γ_{e0}. The obtained maximum positron γ_{e^+} and yield are illustrated in Figs. 5(a) and 5(b). One can see that the final positron energy is proportional to a_0. The linear scaling in accordance with Eq. (1) takes place for $a_0 \geqslant 550$ and $\gamma_{e0} \geqslant 1000$. In other cases, the reflection occurs either before ($a_0 > \gamma_{e0}$) or after the peak ($a_0 \lesssim \gamma_{e0}$). Consequently, the fields at the moment of positron creation are smaller than a_0, leading to lower energies. Simulations confirm the increase of $\mathcal{E}_{\max}$ with a larger focal spot size, e.g., $\mathcal{E}_{\max} = 3.55$ GeV at $w_L = 5.1$ μm ($a_0 = 550$).

The positron yield is essentially governed by the field parameters a_0 and χ_e. For an order of magnitude estimate of the positron yield, we assume that all electrons are reflected, and neglect the energy of the absorbed laser photons $\sim a_0^3\omega_L$ with respect to the much larger electron energy $\gamma_{e0}m$. According to momentum conservation, we have $N_\nu\omega_\nu \sim N_e\gamma_{e0}m$, with the electron and photon numbers N_e and N_ν, respectively, and the emitted photon frequency ω_ν. The pair production probability per laser cycle of a photon colliding with a linearly polarized laser is $P_{e^\pm} \sim \alpha a_0 f(\chi_\nu)$, where the photon quantum nonlinearity parameter is $\chi_\nu \approx 2a_0\omega\omega_\nu/m^2$, and $f(x)$ is a fitting function $f(x) = 0.453K_{1/3}^2(4/3x)/[1 + 0.145x^{1/4}\ln(1 + 2.26x) + 0.33x]$ [84]. Since the radiative energy loss of electrons increases nonlinearly with χ_e, assuming electrons are reflected at the peak of the laser pulse and lose most energies there, we have $\chi_e \approx 2\gamma_{e0}a_0\omega/m$, and the typical energy of the emitted photons is $\omega_\nu \approx \gamma_{e0}m/2$ according to Ref. [84]. Finally, we have a relation that shows only dependence on the initial parameters: $N_{e^\pm} \sim N_\nu P_{e^\pm} \sim N_e\alpha a_0 f(\chi_{e_0}/2)$. According to our 3D PIC simulations, we have the positron yield

$$N_{e^\pm} \approx 3 \times 10^{-3} N_e a_0 f(\chi_{e_0}/2). \quad (2)$$

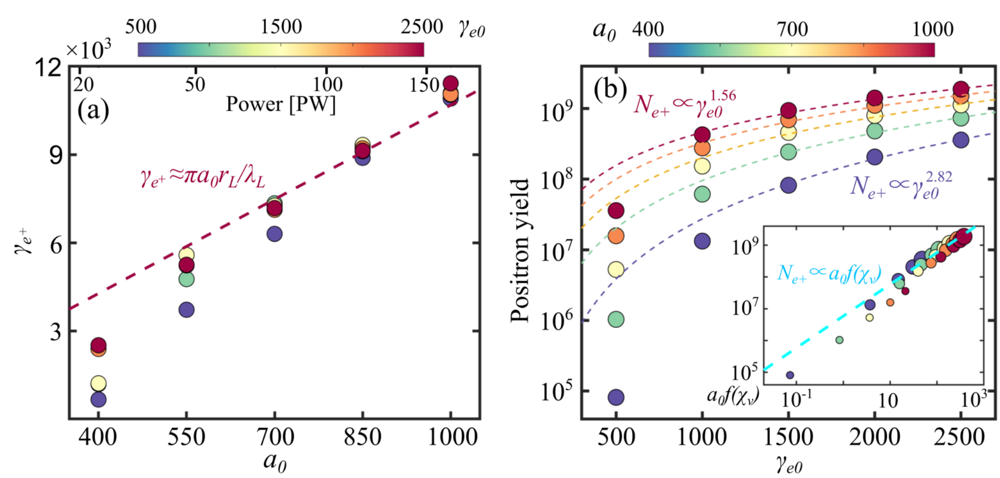

FIG. 5. Scaling of the maximum positron energy γ_{e^+} (a) and yield (b). In (a), the color scale represents the initial electron γ_{e0}, while in (b) the parameter a_0. In the inset of (b), the size of the circles displays their γ_{e0}, $w_L = 3.4$ μm. The inset in (b) demonstrates the scaling (dashed line) with respect to $a_0 f(\chi_\nu)$ given in Eq. (2).

The positron yield increases significantly with a higher a_0 and γ_{e0}, with a linear dependence with respect to $a_0 f(\chi_{e_0}/2)$. At small $a_0 f(\chi_{e_0}/2)$ (small γ_{e0}), Eq. (2) overestimates the yield because $\gamma_{e0} < a_0$ and most electrons are stopped before reaching the peak. Moreover, for the same a_0 and different γ_{e0}, one can obtain very good fittings for larger χ_{e_0} ($\gamma_{e0} \geqslant 1000$). The indices m of the scaling $N_{e^+} \propto \gamma_{e0}^m$ are 2.82, 2.25, 1.91, 1.70, and 1.56 for $a_0 = 400$, 550, 700, 850, and 1000, respectively, in accordance with the function $f(x)$.

For a given power of a laser beam, the acceleration energy is roughly fixed, however, to enhance the positron yield, one may need a beam focusing to increase a_0. For instance, for 10-PW lasers with smaller $w_L = 1.7$ μm, $\mathcal{E}_{\max} \approx 1.6$ GeV, and when selecting $\theta < 10^\circ$, the peak energy 0.8 GeV, charge 0.4 pC, and energy spread ∼30% are achieved. Such high-quality positron sources would have important applications in QED, nuclear, and particle physics.

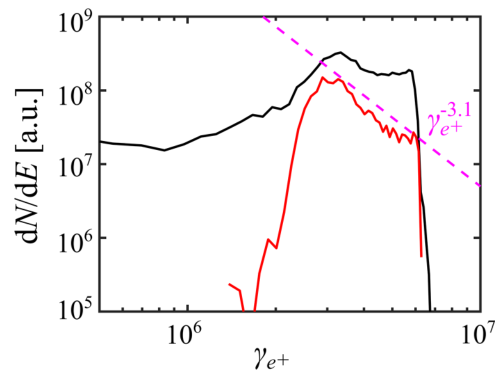

FIG. 6. Positron energy spectra obtained with the astrophysical conditions, where the black and red lines show the spectra selected within a cone of angle 30° and 3° (with respect to the lepton propagation direction), respectively. The purple dashed line show the observed $\gamma_{e^+}^{-3.1}$ power-law dependence.

III. REFLECTION ACCELERATION IN ASTROPHYSICAL SCENARIOS

Motivated by the scaling dependence in Eq. (1), we expect that our mechanism could be effective in astrophysical conditions. In the following, we discuss the scalability of the proposed lepton acceleration mechanism from infrared lasers at μm scales and GeV energies to astrophysical scenarios. We consider a situation when the self-generated fields of the injected electron bunch and collective plasma effects can be neglected as in the laser-driven regime (requiring $n_e/n_c \ll 1$), and the considered mechanism will be valid *irrespective of the wavelength* of the electromagnetic pulses, as long as the dimensionless parameters describing the interaction fulfill $\chi_e, \chi_\nu \sim 1$.

In the universe, there exists strong electromagnetic radiation with frequencies spanning from radio waves to γ-rays. For our acceleration scheme, radio waves are preferable because they could be coherent and at the same field strength, the field parameter a_0 and therefore the acceleration energy is higher than in the case of shorter wavelength. The brightest sources of radio waves discovered up to now are fast radio bursts (FRBs), which recently have attracted great attention due to their extreme luminosity varying from $\mathcal{L} = 10^{38}$ to 10^{46} erg/s [73,85,86]. The observed frequency is usually about 1.4 GHz [87,88], and the pulse duration spans from millisecond to tens of nanoseconds [89]. The radius of FRB sources defined as $R_s \equiv \gamma_s \lambda_w$ is about hundreds of meters [90], where γ_s is the Lorentz factor of the source, and λ_w the wavelength of radiation. The radiation is coherent and is nearly 100% linearly polarized [91,92]. Therefore, FRBs can be treated as loosely focused linearly polarized electromagnetic waves [93,94].

Magnetars are assumed to be responsible for part of the FRBs [73]. The radius of magnetars is about 10 km, and their rotation period is about seconds, leading to a light cylinder region of $r_{\rm LC} \sim 10^4$ km [95], where the last magnetic field line is closed [96]. While the magnetic field at the surface is extremely strong, up to 10^{13}–10^{15} G [97,98], it is negligible near the light cylinder, possibly about several G [99–102]. According to the Goldreich-Juilian charge density, the plasma density $n_{\rm GJ} \sim 10^{12}(B/10^{12}\ \mathrm{G})(P/0.1\ \mathrm{s})^{-1}\,\mathrm{cm}^{-3} \sim 0.1\ \mathrm{cm}^{-3}$ near the light cylinder is negligible [96,103] such that collective plasma effects can be neglected. This region is also a potential site where the FRBs are emitted [92,104]. The wave intensity at this region propagating outwards can be roughly estimated as $I_w \sim \mathcal{L}/(4\pi r_{\rm LC}^2) \lesssim 10^{20}\ \mathrm{W/cm^2}$, corresponding to $a_0 \lesssim 10^7$ and $B_w \lesssim 0.75$ GG.

In this region, the ultrarelativistic radio waves of FRBs emerging from a magnetar [105] could encounter relativistic electrons accelerated to high energies in the magnetosphere, possibly due to electrostatic fields [106,107], which move along the magnetic field lines towards the magnetar core. If the electron energies were $\gamma_{e0} \sim a_0$, the reflection acceleration could work with $\chi_{e0} \sim 1$. Based on the above parameters and our energy scaling Eq. (1), one can estimate that the maximum lepton energy due to reflection acceleration would reach the PeV range, with $w_L \sim 1$ km and $I_w \sim 10^{17}\ \mathrm{W/cm^2}$. This is still smaller than the upper limit of the plane-wave theory of $ma_0^2/2 \approx 40$ PeV. Thus, the reflection acceleration mechanism could contribute to UHECR.

To demonstrate the scalability of the proposed lepton acceleration mechanism to astrophysical scenarios, we have conducted 3D PIC simulations with the parameters listed in Table I.

Here, a relatively small focal spot is considered to reduce the computational resources. Our simulations show that the main physical processes remain the same even for FRB pulses and the reflected positron energy reaches 3.3 TeV because of a much higher a_0, more than one order of magnitude higher than the initial value. Note that here the energy spectrum exhibits a nonthermal power-law dependence $\gamma_{e^+}^{-3.1}$ for the high-energy part by selecting the collimated positrons, as the red line shown in Fig. 6, similar to astrophysical observations [75,108–111]. This power-law spectrum in contrast to the thermal one, is a key feature of the UHECR, with the index of the power law being still an open question despite some astrophysical observations pointing out the index close to −3 [75,108–111].

In principle, without photon emission, electrons can be accelerated to much higher energies or at least the same γ factor as protons, which is at the PeV level. However, on earth, the observed maximum electron energy is only about

TABLE I. Comparison of the typical parameters for reaching our regime in the laboratory and astrophysical scenarios.

	f_{EM}	λ_{EM}	τ_{EM}	B_{EM}	w_{EM}	a_0	γ_e	χ_e
Laser	1.89 PHz	1 μm	25 fs	107 MG	2 μm	550	1000	2.2
FRB	1.4 GHz	1.35 m	33.8 ns	70 G	3.38 m	10^6	5×10^5	1.63

tens of TeV [75]. This has been explained by the photon emission, especially the synchrotron emission over a long distance propagation. The energy loss length of electrons has been widely discussed in astrophysical literature [112]. The lifetime of electrons with energy $\gg$100 TeV is estimated to be less than several hundred years, i.e., they cannot propagate more than a few tens of parsecs ($\sim 3 \times 10^{13}$ km, comparable to the Milky Way diameter) from their acceleration sites. That is why the observed lepton energy is about tens of TeV on earth [113,114].

While the RR dominated reflection regime does not work for ions, if one conjectures that ions are created at rest at the wave peak, they would attain energies exceeding 10^{19}–10^{21} eV depending on the ion species (at the same Lorentz factor of electrons) [115]. This is because for $a_0 \gg M/m$, with the ion mass M, the acceleration progress should be almost identical except for the RR effects. Moreover, the acceleration distance is roughly the distance when the intensity is decreased to half of its peak value. This is only about 10^4–10^5 km, slightly larger than the diameter of earth, but extremely small compared to the galaxy scale. Hence, it might have a much higher probability to work compared to the Fermi acceleration which requires a Mpc (about 10^{19} km) acceleration distance [116].

IV. CONCLUSION

In conclusion, we put forward a lepton acceleration mechanism which occurs when RR effects become dominant. The counterpropagating electrons to an ultrastrong laser beam and the created secondary electrons and positrons can be stopped and reflected at the peak of the laser pulse, and then accelerated to much higher energies than the initial injection energy. While with current laser facilities, the obtained accelerated electron beam quality is difficult to compete with LWFA, the reflection acceleration provides a conceptually simple method to create and accelerate positrons to GeV energies in a single stage which shall be attractive in forthcoming PW facilities such as the 1 PW + 10 PW laser system at SULF, China [117], the 2 × 10 PW laser system at ELI-NP [118], and the 2 × 25 PW OPAL laser system in Rochester, NY, USA [119]. The astrophysical observation data suggest that this acceleration mechanism may contribute to the generation of UHECR emerging from FRBs.

DATA AVAILABILITY

The data that support the findings of this article are not publicly available upon publication because it is not technically feasible and/or the cost of preparing, depositing, and hosting the data would be prohibitive within the terms of this research project. The data are available from the authors upon reasonable request.

APPENDIX: LEPTON ACCELERATION

The electrons leave the laser pulse either in the longitudinal (at small angles relative to the laser propagation direction) or transverse directions (at large angles). For ultrarelativistic electrons with divergence θ, the longitudinal interaction time with the focused laser beam can be estimated as $t_\parallel \sim z_R/\cos\theta$, where $z_R = \pi w_L^2/\lambda_L$ is the Rayleigh length, assuming that the field is significantly damped at $z > z_R$. The transverse interaction time can be estimated as $t_\perp \sim w_L\sqrt{1+z^2/z_R^2}/\sin\theta \sim \sqrt{2}w_L/\sin\theta$. The time to slip from the laser pulse in the longitudinal direction is $t_\parallel^{\mathrm{pulse}} = \tau_L/[2(1-\beta_e\cos\theta)] \approx \tau_L\gamma_e^2/(1+\gamma_e^2\theta^2)$ at $\theta \ll 1$, which is much larger than $t_\parallel$ and $t_\perp$ for our parameters for the given pulse duration τ_L.

Thus, $t_\parallel/t_\perp \sim \pi w_L \tan(\theta)/(\sqrt{2}\lambda_L)$, i.e., at small angles $\theta < \sqrt{2}\lambda_L/(\pi w_L) \ll 1$, the electron leaves the focal volume longitudinally, and vice versa.

The dephasing time in a plane-wave approximation is $t_{\mathrm{dp}} = \pi/[\omega(1-\beta_e\cos\theta)] \approx \lambda_L\gamma_e^2/(1+\gamma_e^2\theta^2)$, which in the focused laser pulse decreases to $t_{\mathrm{dp}} \sim z_R$ at small angles $\theta \ll \sqrt{2}\lambda_L/(\pi w_L) = \sqrt{2}w_L/z_R$ (see Ref. [53]). Thus, at small angles the interaction and dephasing times coincides, which then provides the acceleration time $t_{\mathrm{acc}} \sim z_R$.

At large angles $\theta > \sqrt{2}\lambda_L/(\pi w_L)$, the dephasing time $t_{\mathrm{dp}} \sim \lambda_L\gamma_e^2/(1+\gamma_e^2\theta^2) \sim \lambda_L/\theta^2$ (for $\theta \gtrsim \gamma_e^{-1}$), with $\theta \sim \sqrt{2}w_L/z_R$, and we derive $t_{\mathrm{dp}} \sim \pi z_R/2$, which also coincides with the interaction time in this case $t_\perp \sim \sqrt{2}w_L/\sin\theta \sim t_{\mathrm{acc}}$.

Based on the above discussion, the acceleration time is

$$t_{\mathrm{acc}} \approx \begin{cases} z_R, & \theta \ll \frac{\sqrt{2}\lambda_L}{\pi w_L}, \\ \frac{w_L}{\theta}, & \theta > \frac{\lambda_L}{\pi w_L}. \end{cases} \tag{A1}$$

The θ^{-1} dependence at large angles has been demonstrated by our 3D PIC simulations [see the cyan dashed lines in Figs. 4(c) and 4(d)].

Now we can estimate the energy gain. At small angles $\theta \ll \sqrt{2}\lambda_L/(\pi w_L)$, the energy gain is $\mathcal{E}_{\max} \sim eE_L v_\perp t_\parallel \sim eE_L z_R\theta$, in accordance with pure vacuum laser acceleration such as in Refs. [36,53]. Here, we have assumed therein an average field strength over the optical cycle of $E_L/2$. To give a simple order of magnitude estimation of the attainable maximum energy, we assume a maximum angle $\theta \sim \lambda_L/\pi w_L$, yielding

$$\mathcal{E}_{\max} \sim \pi m a_0 w_L/\lambda_L, \tag{A2}$$

which is presented in Eq. (1). At larger angles $\theta > \sqrt{2}\lambda_L/(\pi w_L)$, we obtain $\mathcal{E}_{\max} \sim eE_L v_\perp t_\perp \sim eE_L w_L$, similar to Eq. (A2).

[1] E. Esarey, E. B. Schroeder, and W. P. Leemans, Physics of laser-driven plasma-based electron accelerators, Rev. Mod. Phys. **81**, 1229 (2009).

[2] A. Pukhov and J. Meyer-ter-Vehn, Laser wake field acceleration: The highly non-linear broken-wave regime, Appl. Phys. B **74**, 355 (2002).

[3] S. Gordienko and A. Pukhov, Scalings for ultrarelativistic laser plasmas and quasimonoenergetic electrons, Phys. Plasmas **12**, 043109 (2005).

[4] W. Lu, M. Tzoufras, C. Joshi, F. S. Tsung, W. B. Mori, J. Vieira, R. A. Fonseca, and L. O. Silva, Generating multi-GeV electron bunches using single stage laser wakefield acceleration in a 3D nonlinear regime, Phys. Rev. ST Accel. Beams **10**, 061301 (2007).

[5] S. Steinke, J. van Tilborg, C. Benedetti, C. G. R. Geddes, C. B. Schroeder, J. Daniels, K. K. Swanson, A. J. Gonsalves, K. Nakamura, N. H. Matlis, B. H. Shaw, E. Esarey, and W. P. Leemans, Multistage coupling of independent laser-plasma accelerators, Nature (London) **530**, 190 (2016).

[6] A. J. Gonsalves, K. Nakamura, J. Daniels, C. Benedetti, C. Pieronek, T. C. H. de Raadt, S. Steinke, J. H. Bin, S. S. Bulanov, J. van Tilborg, *et al.*, Petawatt laser guiding and electron beam acceleration to 8 GeV in a laser-heated capillary discharge waveguide, Phys. Rev. Lett. **122**, 084801 (2019).

[7] A. Golovanov, I. Y. Kostyukov, A. Pukhov, and V. Malka, Energy-conserving theory of the blowout regime of plasma wakefield, Phys. Rev. Lett. **130**, 105001 (2023).

[8] J. Vieira and J. T. Mendonça, Nonlinear laser driven donut wakefields for positron and electron acceleration, Phys. Rev. Lett. **112**, 215001 (2014).

[9] L. Reichwein, A. Pukhov, A. Golovanov, and I. Y. Kostyukov, Positron acceleration via laser-augmented blowouts in two-column plasma structures, Phys. Rev. E **105**, 055207 (2022).

[10] G. J. Cao, C. A. Lindstrøm, E. Adli, S. Corde, and S. Gessner, Positron acceleration in plasma wakefields, Phys. Rev. Accel. Beams **27**, 034801 (2024).

[11] T. Silva, L. Amorim, M. Downer, M. Hogan, V. Yakimenko, R. Zgadzaj, and J. Vieira, Stable positron acceleration in thin, warm, hollow plasma channels, Phys. Rev. Lett. **127**, 104801 (2021).

[12] T. Silva and J. Vieira, Positron acceleration in plasma waves driven by non-neutral fireball beams, Phys. Rev. Accel. Beams **26**, 091301 (2023).

[13] A. S. Firouzjaei and B. Shokri, Trapping and acceleration of hollow electron and positron bunch in a quasi-linear donut wakefield, Phys. Plasmas **24**, 013107 (2017).

[14] M. Streeter, C. Colgan, J. Carderelli, Y. Ma, N. Cavanagh, E. Los, H. Ahmed, A. Antoine, T. Audet, M. Balcazar, *et al.*, Narrow bandwidth, low-emittance positron beams from a laser-wakefield accelerator, Sci. Rep. **14**, 6001 (2024).

[15] Z. Xu, C. Xiao, H. Lu, R. Hu, J. Yu, Z. Gong, Y. Shou, J. Liu, C. Xie, S. Chen, *et al.*, New injection and acceleration scheme of positrons in the laser-plasma bubble regime, Phys. Rev. Accel. Beams **23**, 091301 (2020).

[16] R. Hessami and S. Gessner, Compact source of positron beams with small thermal emittance, Phys. Rev. Accel. Beams **26**, 123402 (2023).

[17] B. Shen and J. Meyer-ter-Vehn, Pair and γ-photon production from a thin foil confined by two laser pulses, Phys. Rev. E **65**, 016405 (2001).

[18] X. Wang, R. Ischebeck, P. Muggli, T. Katsouleas, C. Joshi, W. Mori, and M. Hogan, Positron injection and acceleration on the wake driven by an electron beam format in a foil-and-gas plasma, Phys. Rev. Lett. **101**, 124801 (2008).

[19] X. Wang, P. Muggli, T. Katsouleas, C. Joshi, W. Mori, R. Ischebeck, and M. Hogan, Optimization of positron trapping and acceleration in an electron-beam-driven plasma wakefield accelerator, Phys. Rev. ST Accel. Beams **12**, 051303 (2009).

[20] B. Martinez, B. Barbosa, and M. Vranic, Creation and direct laser acceleration of positrons in a single stage, Phys. Rev. Accel. Beams **26**, 011301 (2023).

[21] J. Zhao, Y.-T. Hu, Y. Lu, H. Zhang, L.-X. Hu, X.-L. Zhu, Z.-M. Sheng, I. C. E. Turcu, A. Pukhov, F.-Q. Shao, *et al.*, All-optical quasi-monoenergetic GeV positron bunch generation by twisted laser fields, Commun. Phys. **5**, 15 (2022).

[22] J. Zhao, Q.-N. Li, Y.-T. Hu, H. Zhang, Y. Cao, R. Sha, F.-Q. Shao, and T.-P. Yu, Terahertz-driven positron acceleration assisted by ultra-intense lasers, Opt. Express **31**, 23171 (2023).

[23] W.-Y. Liu, K. Xue, F. Wan, M. Chen, J.-X. Li, F. Liu, S.-M. Weng, Z.-M. Sheng, and J. Zhang, Trapping and acceleration of spin-polarized positrons from γ photon splitting in wakefields, Phys. Rev. Res. **4**, L022028 (2022).

[24] Z. Xu, L. Yi, B. Shen, J. Xu, L. Ji, T. Xu, L. Zhang, S. Li, and Z. Xu, Driving positron beam acceleration with coherent transition radiation, Commun. Phys. **3**, 191 (2020).

[25] L. I. I. Gamiz, R. Babjak, B. Martinez, and M. Vranić, Improved Bethe–Heitler positron creation and retention by combining direct laser acceleration and solid target interaction within a gas jet, Plasma Phys. Control. Fusion **67**, 055025 (2025).

[26] L. D. Amorim, C. Benedetti, S. S. Bulanov, D. Terzani, A. Huebl, C. B. Schroeder, J.-L. Vay, and E. Esarey, Design study for a compact, two-stage, laser-plasma-based source of positron beams, Plasma Phys. Control. Fusion **65**, 085016 (2023).

[27] H. Fujii, K. Marsh, W. An, S. Corde, M. Hogan, V. Yakimenko, and C. Joshi, Positron beam extraction from an electron-beam-driven plasma wakefield accelerator, Phys. Rev. Accel. Beams **22**, 091301 (2019).

[28] H. Chen, S. Wilks, D. Meyerhofer, J. Bonlie, C. Chen, S. Chen, C. Courtois, L. Elberson, G. Gregori, W. Kruer, *et al.*, Relativistic quasimonoenergetic positron jets from intense laser-solid interactions, Phys. Rev. Lett. **105**, 015003 (2010).

[29] K. Sugimoto, Y. He, N. Iwata, I. Yeh, K. Tangtartharakul, A. Arefiev, and Y. Sentoku, Positron generation and acceleration in a self-organized photon collider enabled by an ultraintense laser pulse, Phys. Rev. Lett. **131**, 065102 (2023).

[30] A. A. Sahai, Quasimonoenergetic laser plasma positron accelerator using particle-shower plasma-wave interactions, Phys. Rev. Accel. Beams **21**, 081301 (2018).

[31] D. Terzani, C. Benedetti, S. S. Bulanov, C. B. Schroeder, and E. Esarey, Compact, all-optical positron production and collection scheme, Phys. Rev. Accel. Beams **26**, 113401 (2023).

[32] C. Adolphsen, D. Angal-Kalinin, T. Arndt, M. Arnold, R. Assmann, B. Auchmann, K. Aulenbacher, A. Ballarino, B. Baudouy, P. Baudrenghien, *et al.*, European strategy for

particle physics–Accelerator R&D roadmap, CERN Yellow Rep. Monogr. **1**, 1 (2022).
[33] P. Musumeci, C. Boffo, S. Bulanov, I. Chaikovska, A. F. Golfe, S. Gessner, J. Grames, R. Hessami, Y. Ivanyushenkov, A. Lankford, *et al.*, Positron sources for future high energy physics colliders, in *Snowmass 2021* (HAL, Seattle, 2022).
[34] G. Sarri, K. Poder, J. Cole, W. Schumaker, A. Di Piazza, B. Reville, T. Dzelzainis, D. Doria, L. Gizzi, G. Grittani, *et al.*, Generation of neutral and high-density electron–positron pair plasmas in the laboratory, Nat. Commun. **6**, 6747 (2015).
[35] E. Esarey, P. Sprangle, and J. Krall, Laser acceleration of electrons in vacuum, Phys. Rev. E **52**, 5443 (1995).
[36] Y. I. Salamin and C. H. Keitel, Electron acceleration by a tightly focused laser beam, Phys. Rev. Lett. **88**, 095005 (2002).
[37] V. Marceau, A. April, and M. Piché, Electron acceleration driven by ultrashort and nonparaxial radially polarized laser pulses, Opt. Lett. **37**, 2442 (2012).
[38] J. Powell, S. W. Jolly, S. Vallières, F. Fillion-Gourdeau, S. Payeur, S. Fourmaux, M. Lytova, M. Piché, H. Ibrahim, S. MacLean, and F. Légaré, Relativistic electrons from vacuum laser acceleration using tightly focused radially polarized beams, Phys. Rev. Lett. **133**, 155001 (2024).
[39] M. Thévenet, A. Leblanc, S. Kahaly, H. Vincenti, A. Vernier, F. Quéré, and J. Faure, Vacuum laser acceleration of relativistic electrons using plasma mirror injectors, Nat. Phys. **12**, 355 (2016).
[40] P. K. Singh, F. Y. Li, C. K. Huang, A. Moreau, R. Hollinger, A. Junghans, A. Favalli, C. Calvi, S. Wang, Y. Wang, H. Song, J. J. Rocca, R. E. Reinovsky, and S. Palaniyappan, Vacuum laser acceleration of super-ponderomotive electrons using relativistic transparency injection, Nat. Commun. **13**, 54 (2022).
[41] A. De Andres, S. Bhadoria, J. T. Marmolejo, A. Muschet, P. Fischer, H. Reza Barzegar, T. Blackburn, A. Gonoskov, D. Hanstorp, M. Marklund, and L. Veisz, Unforeseen advantage of looser focusing in vacuum laser acceleration, Commun. Phys. **7**, 293 (2024).
[42] P. H. Bucksbaum, M. Bashkansky, and T. J. McIlrath, Scattering of electrons by intense coherent light, Phys. Rev. Lett. **58**, 349 (1987).
[43] F. V. Hartemann, S. N. Fochs, G. P. Le Sage, N. C. Luhmann, J. G. Woodworth, M. D. Perry, Y. J. Chen, and A. K. Kerman, Nonlinear ponderomotive scattering of relativistic electrons by an intense laser field at focus, Phys. Rev. E **51**, 4833 (1995).
[44] V. Malka, E. Lefebvre, and J. L. Miquel, Experimental observation of electrons accelerated in vacuum to relativistic energies by a high-intensity laser, Phys. Rev. Lett. **78**, 3314 (1997).
[45] P. Mora and B. Quesnel, Comment on "experimental observation of electrons accelerated in vacuum to relativistic energies by a high-intensity laser", Phys. Rev. Lett. **80**, 1351 (1998).
[46] B. Quesnel and P. Mora, Theory and simulation of the interaction of ultraintense laser pulses with electrons in vacuum, Phys. Rev. E **58**, 3719 (1998).
[47] G. V. Stupakov and M. S. Zolotorev, Ponderomotive laser acceleration and focusing in vacuum for generation of attosecond electron bunches, Phys. Rev. Lett. **86**, 5274 (2001).
[48] F. He, W. Yu, P. Lu, H. Xu, L. Qian, B. Shen, X. Yuan, R. Li, and Z. Xu, Ponderomotive acceleration of electrons by a tightly focused intense laser beam, Phys. Rev. E **68**, 046407 (2003).
[49] C. I. Moore, A. Ting, S. J. McNaught, J. Qiu, H. R. Burris, and P. Sprangle, A laser-accelerator injector based on laser ionization and ponderomotive acceleration of electrons, Phys. Rev. Lett. **82**, 1688 (1999).
[50] S. X. Hu and A. F. Starace, GeV electrons from ultraintense laser interaction with highly charged ions, Phys. Rev. Lett. **88**, 245003 (2002).
[51] A. Di Piazza, C. Müller, K. Z. Hatsagortsyan, and C. H. Keitel, Extremely high-intensity laser interactions with fundamental quantum systems, Rev. Mod. Phys. **84**, 1177 (2012).
[52] I. Y. Dodin and N. J. Fisch, Relativistic electron acceleration in focused laser fields after above-threshold ionization, Phys. Rev. E **68**, 056402 (2003).
[53] A. Maltsev and T. Ditmire, Above threshold ionization in tightly focused, strongly relativistic laser fields, Phys. Rev. Lett. **90**, 053002 (2003).
[54] D. F. Gordon, J. P. Palastro, and B. Hafizi, Superponderomotive regime of tunneling ionization, Phys. Rev. A **95**, 033403 (2017).
[55] A. Yandow, T. Toncian, and T. Ditmire, Direct laser ion acceleration and above-threshold ionization at intensities from 10^{21} W/cm^2 to 3×10^{23} W/cm^2, Phys. Rev. A **100**, 053406 (2019).
[56] A. Yandow, T. N. Ha, C. Aniculaesei, H. L. Smith, C. G. Richmond, M. M. Spinks, H. J. Quevedo, S. Bruce, M. Darilek, C. Chang, D. A. Garcia, E. Gaul, M. E. Donovan, B. M. Hegelich, and T. Ditmire, Above-threshold ionization at laser intensity greater than 10^{20} W/cm^2, Phys. Rev. A **109**, 023119 (2024).
[57] J. W. Yoon, Y. G. Kim, I. W. Choi, J. H. Sung, H. W. Lee, S. K. Lee, and C. H. Nam, Realization of laser intensity over 10^{23} W/cm^2, Optica **8**, 630 (2021).
[58] A. M. Fedotov, N. V. Elkina, E. G. Gelfer, N. B. Narozhny, and H. Ruhl, Radiation friction versus ponderomotive effect, Phys. Rev. A **90**, 053847 (2014).
[59] K. Poder, M. Tamburini, G. Sarri, A. Di Piazza, S. Kuschel, C. D. Baird, K. Behm, S. Bohlen, J. M. Cole, D. J. Corvan, M. Duff, E. Gerstmayr, C. H. Keitel, K. Krushelnick, S. P. D. Mangles, P. McKenna, C. D. Murphy, Z. Najmudin, C. P. Ridgers, G. M. Samarin, *et al.*, Experimental signatures of the quantum nature of radiation reaction in the field of an ultraintense laser, Phys. Rev. X **8**, 031004 (2018).
[60] J. M. Cole, K. T. Behm, E. Gerstmayr, T. G. Blackburn, J. C. Wood, C. D. Baird, M. J. Duff, C. Harvey, A. Ilderton, A. S. Joglekar, K. Krushelnick, S. Kuschel, M. Marklund, P. McKenna, C. D. Murphy, K. Poder, C. P. Ridgers, G. M. Samarin, G. Sarri, D. R. Symes, *et al.*, Experimental evidence of radiation reaction in the collision of a high-intensity laser pulse with a laser-wakefield accelerated electron beam, Phys. Rev. X **8**, 011020 (2018).
[61] X. Geng, L. Ji, B. Shen, B. Feng, Z. Guo, Q. Yu, L. Zhang, and Z. Xu, Quantum reflection above the classical radiation-reaction barrier in the quantum electro-dynamics regime, Commun. Phys. **2**, 66 (2019).
[62] Z. Gong, R. Hu, J. Yu, Y. Shou, A. Arefiev, and X. Yan, Radiation rebound and quantum splash in electron-laser collisions, Phys. Rev. Accel. Beams **22**, 093401 (2019).

[63] A. Griffith, K. Qu, and N. J. Fisch, Particle deceleration for collective QED signatures, Phys. Plasmas **29**, 073104 (2022).

[64] M. Mirzaie, C. I. Hojbota, D. Y. Kim, V. B. Pathak, T. G. Pak, C. M. Kim, H. W. Lee, J. W. Yoon, S. K. Lee, Y. J. Rhee, *et al.*, All-optical nonlinear Compton scattering performed with a multi-petawatt laser, Nat. Photon. **18**, 1212 (2024).

[65] V. I. Ritus, Quantum effects of the interaction of elementary particles with an inense electromagnetic field, J. Sov. Laser Res. **6**, 497 (1985).

[66] D. L. Burke, R. C. Field, G. Horton-Smith, J. E. Spencer, D. Walz, S. C. Berridge, W. M. Bugg, K. Shmakov, A. W. Weidemann, C. Bula, K. T. McDonald, E. J. Prebys, C. Bamber, S. J. Boege, T. Koffas, T. Kotseroglou, A. C. Melissinos, D. D. Meyerhofer, D. A. Reis, and W. Ragg, Positron production in multiphoton light-by-light scattering, Phys. Rev. Lett. **79**, 1626 (1997).

[67] Z. Bu, L. Ji, S. Lei, H. Hu, X. Zhang, and B. Shen, Twisted Breit-Wheeler electron-positron pair creation via vortex gamma photons, Phys. Rev. Res. **3**, 043159 (2021).

[68] A. Eckey, A. Golub, F. C. Salgado, S. Villalba-Chávez, A. B. Voitkiv, M. Zepf, and C. Müller, Impact of laser focusing and radiation reaction on particle spectra from nonlinear Breit-Wheeler pair production in the nonperturbative regime, Phys. Rev. A **110**, 043113 (2024).

[69] A. Di Piazza, K. Z. Hatsagortsyan, and C. H. Keitel, Strong signatures of radiation reaction below the radiation-dominated regime, Phys. Rev. Lett. **102**, 254802 (2009).

[70] J.-X. Li, K. Z. Hatsagortsyan, B. J. Galow, and C. H. Keitel, Attosecond gamma-ray pulses via nonlinear Compton scattering in the radiation-dominated regime, Phys. Rev. Lett. **115**, 204801 (2015).

[71] J.-X. Li, Y.-Y. Chen, K. Z. Hatsagortsyan, and C. H. Keitel, Single-shot carrier-envelope phase determination of long superintense laser pulses, Phys. Rev. Lett. **120**, 124803 (2018).

[72] K.-H. Zhuang, Y.-Y. Chen, Y.-F. Li, K. Z. Hatsagortsyan, and C. H. Keitel, Laser-driven lepton polarization in the quantum radiation-dominated reflection regime, Phys. Rev. D **108**, 033001 (2023).

[73] B. Zhang, The physics of fast radio bursts, Rev. Mod. Phys. **95**, 035005 (2023).

[74] T. Piran, The physics of gamma-ray bursts, Rev. Mod. Phys. **76**, 1143 (2005).

[75] A. Letessier-Selvon and T. Stanev, Ultrahigh energy cosmic rays, Rev. Mod. Phys. **83**, 907 (2011).

[76] J.-L. Vay, A. Almgren, J. Bell, L. Ge, D. Grote, M. Hogan, O. Kononenko, R. Lehe, A. Myers, C. Ng, J. Park, R. Ryne, O. Shapoval, M. Thévenet, and W. Zhang, Warp-X: A new exascale computing platform for beam–plasma simulations, Nucl. Instrum. Methods Phys. Res. Sect. A **909**, 476 (2018).

[77] B. M. Cowan, D. L. Bruhwiler, J. R. Cary, E. Cormier-Michel, and C. G. R. Geddes, Generalized algorithm for control of numerical dispersion in explicit time-domain electromagnetic simulations, Phys. Rev. ST Accel. Beams **16**, 041303 (2013).

[78] To improve accuracy and suppress numerical Cherenkov radiation, we employed the modified finite-difference Maxwell equations solver CKC, and the pseudospectral Maxwell equations solver PSATD, which gave comparable results. Numerical convergence has been checked by doubling the resolution in both longitudinal and transverse directions. We found that both the initial self-fields and the effect of beam charge and current on evolving fields can be neglected because of the dominance of the laser field.

[79] A. Gonoskov, T. Blackburn, M. Marklund, and S. Bulanov, Charged particle motion and radiation in strong electromagnetic fields, Rev. Mod. Phys. **94**, 045001 (2022).

[80] F. Lureau, G. Matras, O. Chalus, C. Derycke, T. Morbieu, C. Radier, O. Casagrande, S. Laux, S. Ricaud, G. Rey, *et al.*, High-energy hybrid femtosecond laser system demonstrating 2×10 PW capability, High Power Laser Sci. Eng. **8**, e43 (2020).

[81] H. Li, K. Liu, X. Wang, X. Liu, X. Meng, Y. Liu, L. Song, Y. Leng, and R. Li, Timing fluctuation correction for the front end of a 100-PW laser, High Power Laser Sci. Eng. **11**, e52 (2023).

[82] Z. Li, Y. Leng, and R. Li, Further development of the short-pulse petawatt laser: Trends, technologies, and bottlenecks, Laser Photon. Rev. **17**, 2100705 (2023).

[83] C. Thaury, F. Quere, J.-P. Geindre, A. Levy, T. Ceccotti, P. Monot, M. Bougeard, F. Réau, P. d'Oliveira, P. Audebert, *et al.*, Plasma mirrors for ultrahigh-intensity optics, Nat. Phys. **3**, 424 (2007).

[84] T. Blackburn, A. Ilderton, C. Murphy, and M. Marklund, Scaling laws for positron production in laser–electron-beam collisions, Phys. Rev. A **96**, 022128 (2017).

[85] J. M. Cordes and S. Chatterjee, Fast radio bursts: An extragalactic enigma, Annu. Rev. Astron. Astrophys. **57**, 417 (2019).

[86] B. Zhang, The physical mechanisms of fast radio bursts, Nature (London) **587**, 45 (2020).

[87] A. Lyne and F. Graham-Smith, *Pulsar Astronomy*, Cambridge Astrophysics Series No. 48 (Cambridge University Press, Cambridge, UK, 2012).

[88] B. Zhang, Fast radio burst energetics and detectability from high redshifts, Astrophys. J. Lett. **867**, L21 (2018).

[89] K. Nimmo, J. Hessels, F. Kirsten, A. Keimpema, J. Cordes, M. Snelders, D. Hewitt, R. Karuppusamy, A. Archibald, V. Bezrukovs, *et al.*, Burst timescales and luminosities as links between young pulsars and fast radio bursts, Nat. Astron. **6**, 393 (2022).

[90] P. Kumar, W. Lu, and M. Bhattacharya, Fast radio burst source properties and curvature radiation model, Mon. Not. R. Astron. Soc. **468**, 2726 (2017).

[91] V. Gajjar, A. Siemion, D. Price, C. Law, D. Michilli, J. Hessels, S. Chatterjee, A. Archibald, G. Bower, C. Brinkman, *et al.*, Highest frequency detection of FRB 121102 at 4–8 GHz using the Breakthrough Listen digital backend at the Green Bank Telescope, Astrophys. J. **863**, 2 (2018).

[92] Y. Lyubarsky, Fast radio bursts from reconnection in a magnetar magnetosphere, Astrophys. J. **897**, 1 (2020).

[93] M. Popov, A. Rudnitskii, and V. Soglasnov, Giant pulses of the Crab Nebula pulsar as an indicator of a strong electromagnetic wave, Astron. Rep. **61**, 178 (2017).

[94] Y.-P. Yang and B. Zhang, Fast radio bursts as strong waves interacting with the ambient medium, Astrophys. J. Lett. **892**, L10 (2020).

[95] M. Lyutikov, Magnetic loading of magnetars' flares, Mon. Not. R. Astron. Soc. **509**, 2689 (2021).
[96] P. Goldreich and W. H. Julian, Pulsar electrodynamics, Astrophys. J. **157**, 869 (1969).
[97] J. Katz, Physical processes in gamma-ray bursts, Astrophys. J. **260**, 371 (1982).
[98] R. C. Duncan and C. Thompson, Formation of very strongly magnetized neutron stars-implications for gamma-ray bursts, Astrophys. J. Lett. **392**, L9 (1992).
[99] S. E. Gralla, A. Lupsasca, and A. Philippov, Inclined pulsar magnetospheres in general relativity: Polar caps for the dipole, quadrudipole, and beyond, Astrophys. J. **851**, 137 (2017).
[100] C. Kalapotharakos, Z. Wadiasingh, A. K. Harding, and D. Kazanas, The multipolar magnetic field of the millisecond pulsar PSR J0030+ 0451, Astrophys. J. **907**, 63 (2021).
[101] J. Petri, Multipolar electromagnetic fields around neutron stars: Exact vacuum solutions and related properties, Mon. Not. R. Astron. Soc. **450**, 714 (2015).
[102] J. Pétri, Radiation from an off-centred rotating dipole in vacuum, Mon. Not. R. Astron. Soc. **463**, 1240 (2016).
[103] A. Philippov and M. Kramer, Pulsar magnetospheres and their radiation, Annu. Rev. Astron. Astrophys. **60**, 495 (2022).
[104] B. Zhang, Coherent inverse Compton scattering by bunches in fast radio bursts, Astrophys. J. **925**, 53 (2022).
[105] V. M. Kaspi and A. M. Beloborodov, Magnetars, Annu. Rev. Astron. Astrophys. **55**, 261 (2017).
[106] W. Lu, P. Kumar, and B. Zhang, A unified picture of galactic and cosmological fast radio bursts, Mon. Not. R. Astron. Soc. **498**, 1397 (2020).
[107] Z. Wadiasingh and A. Timokhin, Repeating fast radio bursts from magnetars with low magnetospheric twist, Astrophys. J. **879**, 4 (2019).
[108] S. Gabici, C. Evoli, D. Gaggero, P. Lipari, P. Mertsch, E. Orlando, A. Strong, and A. Vittino, The origin of galactic cosmic rays: Challenges to the standard paradigm, Int. J. Mod. Phys. D **28**, 1930022 (2019).
[109] F. Fiuza, G. Swadling, A. Grassi, H. Rinderknecht, D. Higginson, D. Ryutov, C. Bruulsema, R. Drake, S. Funk, S. Glenzer, *et al.*, Electron acceleration in laboratory-produced turbulent collisionless shocks, Nat. Phys. **16**, 916 (2020).
[110] S. R. Totorica, T. Abel, and F. Fiuza, Nonthermal electron energization from magnetic reconnection in laser-driven plasmas, Phys. Rev. Lett. **116**, 095003 (2016).
[111] C. Evoli, E. Amato, P. Blasi, and R. Aloisio, Stochastic nature of galactic cosmic-ray sources, Phys. Rev. D **104**, 123029 (2021).
[112] F. A. Aharonian, *Very High Energy Cosmic Gamma Radiation* (World Scientific, Singapore, 2004).
[113] A. Archer, W. Benbow, R. Bird, R. Brose, M. Buchovecky, J. Buckley, V. Bugaev, M. Connolly, W. Cui, M. Daniel, *et al.*, Measurement of cosmic-ray electrons at TeV energies by VERITAS, Phys. Rev. D **98**, 062004 (2018).
[114] S. Recchia, S. Gabici, F. Aharonian, and J. Vink, Local fading accelerator and the origin of TeV cosmic ray electrons, Phys. Rev. D **99**, 103022 (2019).
[115] A. Aab, P. Abreu, M. Aglietta, J. M. Albury, I. Allekotte, A. Almela, J. A. Castillo, J. Alvarez-Muñiz, R. A. Batista, G. A. Anastasi, *et al.*, Features of the energy spectrum of cosmic rays above 2.5×10^{18} eV using the Pierre Auger Observatory, Phys. Rev. Lett. **125**, 121106 (2020).
[116] L. O. Drury, Acceleration of cosmic rays, Contemp. Phys. **35**, 231 (1994).
[117] Z. Gan, L. Yu, C. Wang, Y. Liu, Y. Xu, W. Li, S. Li, L. Yu, X. Wang, X. Liu, *et al.*, The Shanghai Superintense Ultrafast Laser Facility (SULF) project, in *Progress in Ultrafast Intense Laser Science XVI* (Springer, Berlin, 2021), pp. 199–217.
[118] C. Radier, O. Chalus, M. Charbonneau, S. Thambirajah, G. Deschamps, S. David, J. Barbe, E. Etter, G. Matras, S. Ricaud, *et al.*, 10 PW peak power femtosecond laser pulses at ELI-NP, High Power Laser Sci. Eng. **10**, e21 (2022).
[119] J. Bromage III, S.-W. Bahk, M. Bedzyk, I. Begishev, S. Bucht, C. Dorrer, C. Feng, C. Jeon, C. Mileham, R. Roides, *et al.*, MTW-OPAL: A technology development platform for ultra-intense optical parametric chirped-pulse amplification systems, High Power Laser Sci. Eng. **9**, e63 (2021).